Atmos. Meas. Tech. Discuss., 4, 6811–6844, 2011
www.atmos-meas-tech-discuss.net/4/6811/2011/
doi:10.5194/amtd-4-6811-2011

Atmospheric Measurement Techniques Discussions

1-D-Var retrieval of daytime total columnar water vapour from MERIS measurements

R. Lindstrot[1], **R. Preusker**[1], **H. Diedrich**[1], **L. Doppler**[1], **R. Bennartz**[2], **and J. Fischer**[1]

[1]Institut für Weltraumwissenschaften, Freie Universität Berlin, Carl-Heinrich-Becker-Weg 6–10, 12165 Berlin, Germany
[2]Department of Atmospheric and Oceanic Sciences, University of Wisconsin-Madison, 1225 W. Dayton Street Madison, WI, USA

Received: 30 September 2011 – Accepted: 27 October 2011 – Published: 8 November 2011

Correspondence to: R. Lindstrot (rasmus.lindstrot@wew.fu-berlin.de)

Published by Copernicus Publications on behalf of the European Geosciences Union.

Abstract

A new scheme for the retrieval of total columnar water vapour from measurements of MERIS (Medium Resolution Imaging Spectrometer) on ENVISAT (ENVIronmental SATellite) is presented. The algorithm is based on a fast forward model of the water vapour transmittance around 900 nm, including a correction for atmospheric scattering. It provides the water vapour column amount for cloud-free scenes above land and ocean at a spatial resolution of 0.25 km × 0.3 km and 1 km × 1.2 km, depending on whether applied to the "full resolution" or the operational "reduced resolution" mode of MERIS. Uncertainties are provided on a pixel-by-pixel basis, taking into account all relevant sources of error. An extensive validation against various sources of ground-based reference data reveals a high accuracy of MERIS water vapour above land (root mean square deviations between 1mm and 2.7 mm), apart from a wet bias of MERIS between 5 and 10 % that is found in all comparison studies. This wet bias might be caused by spectroscopic uncertainties, such as the description of the water vapour continuum. Above ocean the accuracy is reduced, due to the uncertainty introduced by the unknown atmospheric scattering. Consequently, an increased root mean square deviation of ≥5 mm was found by comparing MERIS total columnar water vapour above ocean against SSM/I and ENVISAT MWR data. An increased wet bias of 2–3 mm is found over ocean, potentially du to a not properly working atmospheric correction scheme.

1 Introduction

1.1 Background

Due to the tremendous importance of water vapour for the greenhouse effect and the energy balance of the earth, the spaceborne monitoring of water vapour column amounts and vertical profiles has a long history in remote sensing. As the water

AMTD
4, 6811–6844, 2011

molecule absorbs electromagnetic radiation ranging from microwave to visible wavelengths, a number of different methods have been developed during the past decades, either making use of either active (e.g. Heise et al., 2006) or passive microwave measurements (e.g. SSM/I (e.g. Schlüssel and Emery, 1990) or mid- and long-wavelength infrared spectral range (e.g. AIRS (Susskind et al., 2003) or IASI (Pougatchev et al., 2009)) or based on sensing the absorption of water vapour in the visible (e.g. GOME (Noël et al., 2002)) or near infrared spectral range from MERIS or MODIS (e.g. Bennartz and Fischer, 2001; Albert et al., 2005; Gao and Kaufman, 2003). Above ocean, microwave and infrared techniques have proven to be superior, due to the well known emissivity and temperature of the ocean surface. Over land, the water vapour signal at these wavelengths is blurred by the uncertain emissivity of the surface, limiting its main applicability to the sensing of upper-air humidity by using strongly absorbing bands. In the visible and near infrared spectral regions, the situation is reversed as the brighter land surfaces allow water vapour retrievals with a higher accuracy as compared to dark water surfaces, where the signal strongly depends on the uncertain influence of scattering in the atmosphere. The $\rho\sigma\tau$-absorption band between 0.9 µm and 1 µm is particularly well suited for water vapour sensing, due to the fact that all land surface types are bright at this spectral range. A number of spectrometers employed currently and in future, such as the Moderate Resolution Imaging Spectroradiometer (MODIS) or the Medium Resolution Imaging Spectrometer (MERIS) and their follow up models, provide measurements in spectral bands within and close-by this water vapour absorption band, allowing for the exploitation of the differential absorption.

1.2 The Medium Resolution Imaging Spectrometer (MERIS)

MERIS is a programmable, medium-spectral resolution, imaging spectrometer (Rast et al., 1999). It is one of ten core instruments on the polar orbiter ENVISAT (**Envi**ronmental **Sat**ellite, launched on 1 March 2002) flying at 800 km in a sun-synchronous orbit with an equator crossing time of 10:30 a.m., descending node, and 98.5° inclination. MERIS consists of 5 identical pushbroom imaging spectrometers

AMTD
4, 6811–6844, 2011

operating in the solar spectral range (390 to 1040 nm), arranged in a fan shape configuration which covers a total field of view of 68.5° and spans a swath width of around 1150 km. The spectral dispersion is achieved by mapping the entrance slit of a grating spectrometer onto a CCD array. The integration time, instrument optics and CCD array resolution are adjusted such that MERIS has a spatial resolution of 260 m × 300 m and a spectral sampling of 1.25 nm. The instrument electronic data rate provides 15 channels which are programmable by ground command in width and in position. In the regular operation mode the spatial resolution is reduced by a factor of 4 along and across track ("reduced resolution" mode). In the "full resolution" mode, the full spatial resolution is transmitted. The central wavelengths of the spectral channels as listed in Table 1 vary slightly across the field of view of MERIS. This "spectral smile" is caused by curvature of the image of the slit formed in the focal plane array, resulting in viewing angle-dependent central wavelengths of the spectral MERIS channels.

2 Physical background of the retrieval method

The absorption of electromagnetic radiation by water vapour, occuring at characteristic wavelengths throughout the solar and terrestrial spectrum, is related to the excitation of various combinations of the three fundamental vibrational modes of the water molecule. Measurements of the reflected sun light within the resulting absorption bands enable a determination of the total columnar water vapour (hereafter referred to as TCWV), provided that

1. incoming solar radiation is available, precluding night-time retrievals,
2. the channel used is located in a non-saturated and therefore sufficiently sensitive part of the absorption band,
3. the optical thickness of other atmospheric species is either zero or precisely known,

AMTD
4, 6811–6844, 2011

4. the surface albedo is known or can be accurately estimated,

5. the paths of the detected photons through the atmosphere are either known to a sufficient degree or predominantly attributable to the unscattered, surface-reflected fraction,

6. the lower troposphere, holding the main part of TCWV, is not obscured by clouds or optically thick aerosol layers.

For monochromatic radiation, the transmittance T through a medium can be related to its optical depth τ and the airmass μ, following the Beer-Lambert law:

$$T = \exp(-\tau/\mu) \quad (1)$$

Neglecting scattering processes and assuming non-saturated absorption, the mass of the absorbing species can thus be directly related to the logarithm of the traversed medium's transmittance. Since the transmittance cannot be measured directly from space, it is approximated by the ratio of two neighbouring bands with differing optical depth. Fischer (1988) proposed to use two closely spaced bands, with one channel located in the in the shortwave end of the $\rho\sigma\tau$-absorption band around 900 nm and the other one in the atmospheric window region around 885 nm. At this spectral range, almost all land surfaces such as vegetated, bare soil or snow-covered areas, are bright and therefore provide a good background for retrievals of total columnar amounts of water vapour. The small spectral distance of merely 15 nm minimizes the difference in surface reflectance and atmospheric scattering properties between the two bands. Finally, by locating the absorption channel at 900 nm instead of sensing higher optical depths of water vapour at e.g. 950 nm, it is assured that the measurements are sensitive to TCWV throughout the range of globally occurring water vapour column amounts. This is due to the fact that the water vapour absorption at 900 nm does not get saturated, even in case of high airmasses in a humid atmosphere. Therefore, the MERIS bands (see Table 1) are perfectly suited for the daytime, cloud-free retrieval of TCWV over land.

AMTD
4, 6811–6844, 2011

Around 900 nm, the ocean surface is dark, except for observing geometries featuring direct, specular reflection of sun light. One therefore has to accept a reduced accuracy of the derived TCWV over ocean due to the stronger impact of atmospheric scattering on the measured band ratio.

3 1-D-Var retrieval algorithm

Since the retrieval algorithm is required to provide

1. flexibility regarding the inclusion of auxiliary information such as background knowledge about aerosol loading, the temperature profile, surface pressure or surface reflectance and
2. uncertainty estimates on a pixel-by-pixel basis,

the inversion of the MERIS measurements is carried out by one-dimensional variational analysis (1-D-Var), instead of relying on e.g. non-linear regression approaches such as artificial neural networks. The drawback of this solution is a considerable increase in computing time, necessitating a fast forward simulation module.

The retrieval scheme is divided into several individual steps, starting with a determination of the surface reflectance in MERIS bands 14 and 15 and a subsequent iterative optimization of TCWV by minimizing the cost function, represented by the absolute difference between the modelled and observed ratios of MERIS bands 15 and 14. In order to account for the influence of scattering on the measured water vapour transmittance, a scattering correction factor is calculated at each retrieval step, depending on the aerosol loading, surface reflectance, viewing geometry and TCWV itself. The uncertainty of the retrieved value of TCWV is calculated after the final iteration step, by taking into account uncertainties introduced by instrumental effects such as sensor noise and uncertainties in prior knowledge of the influencing parameters such as

AMTD
4, 6811–6844, 2011

surface albedo, aerosol optical depth, aerosol scale height, temperature profile and surface pressure. The individual retrieval steps are detailed in the following sections.

3.1 Forward model

In the near infrared spectral range, the remotely sensable information about TCWV is the water vapour transmittance along the light path. Due to the spectral distance of MERIS bands 14 and 15, mainly noticeable through differences in surface reflectance and solar incoming irradiance, and the influence of atmospheric scattering, the measured ratio of the radiances L_i, $R = L_{15}/L_{14}$, deviates from the actual water vapour transmittance. The deviation is a function of the surface albedo and its spectral dependency, the viewing and illumination geometry and the vertical distribution and optical properties of the atmospheric scatterers. In a first step, the measured band ratio R is therefore normalized by the ratio of the solar incoming irradiance E_i at the particular wavelengths of both channels: $R_N = L_{15}/L_{14} * E_{14}/E_{15}$, taking into account the spectral smile effect, causing the central wavelength of MERIS bands to depend slightly on the viewing angle (e.g. Delwart et al., 2007; Lindstrot et al., 2010). Afterwards, R_N is simulated by the ratio of the water vapour transmittance in both bands, corrected for the spectral surface albedo difference and scattering processes in the atmosphere:

A fast forward model of the normalized band ratio R_N as a function of TCWV, the viewing geometry, and the surface albedo, temperature and pressure is needed for the optimization of TCWV. It uses stored absorption coefficients that were calculated with an advanced k-distribution method (Bennartz and Fischer, 2000), based on resorting the large number of quasi-monochromatic spectral intervals within each MERIS band with respect to their optical depth and combining them to a significantly lower number of pseudo-spectral intervals. For a given observing geometry and TCWV, the transmittance T in each MERIS band is modelled by

1. adjusting the tabulated optical depth τ_{ij} for each pseudo-spectral interval i and vertical layer j to match the desired value of TCWV, as it was pre-calculated for fixed values of TCWV,

AMTD
4, 6811–6844, 2011

2. calculating the transmittance in each pseudo-spectral interval from the sum of the optical depth along the line of sight following formula 1 and

3. subsequently summing up all transmittance values with respect to the weights w_i associated to the pseudo-spectral intervals:

$$T = \sum_{i=1}^{\#\text{intervals}} w_i * \exp(-\sum_{j=1}^{\#\text{layers}} \tau_{ij}/\mu) \quad (2)$$

The optical depth values τ_{ij} are stored in look-up tables for 6 standard temperature profiles (McClatchey et al., 1972) and 27 different pressure levels. In order to account for the temperature- and pressure-dependence of the absorption lines, the transmittance is calculated for the four look-up table grid points closest to the actual surface pressure and temperature of the considered scene, hereby assuming that the surface temperature is highly correlated with the actual vertical temperature profile. The final transmittances of MERIS bands 14 and 15 are then calculated as a weighted average among these 4 figures.

As a next step, for land scenes the transmittance ratio is corrected for the difference in spectral surface reflectance. As the true surface reflectance at the MERIS wavelengths is unknown, it is estimated by correcting the measured reflectance at the top of the atmosphere (TOA) for the scattering component, using a look-up table approach for the atmospheric correction. As this procedure is possible only in window channels, the surface albedo at 900 nm is linearly extrapolated from $\alpha_{865\,\text{nm}}$ and $\alpha_{885\,\text{nm}}$. The atmospheric correction relies on assumptions about the aerosol loading, type and vertical distribtion. However, over the relatively bright land surfaces the influence on the surface reflectance retrieval is weak, at least if absolute accuracy is not an issue but the primary goal is to determine the spectral slope in surface reflectance between the closely spaced MERIS bands. The albedo retrieval over land can thus be performed using climatological mean values in case there is no additional information available.

AMTD
4, 6811–6844, 2011

Above the dark ocean the situation is different as there is no spectral dependency of the surface reflectance, however, the influence of atmospheric scattering on the measured band ratio is much more pronounced. Here, the surface reflectance can be simulated using the wind speed for parameterizing the sea surface roughness (Cox and Munk, 1954; Koepke, 1984).

Finally, in order to correct the simulated transmittance ratio for the influence of atmospheric scattering, a scattering correction factor f is extracted from tabulated radiative transfer simulations, using the Matrix Operator Model (MOMO, Fischer and Grassl, 1984; Fell and Fischer, 2001). f represents the relation between pure transmittance T_{noscat}, assuming a non-scattering atmosphere, and the true transmittance T, calculated with MOMO including atmospheric scattering at molecules and particles: $f = T/T_{\text{noscat}}$. f is larger than one, as atmospheric scattering through reflection of incoming solar radiation altogether causes a shortening of the average photon path length in the atmosphere and reduces the amount of water vapour along the photon path by preventing a fraction of photons from traversing the humid boundary layer. Figure 1 shows f and the equivalent error in retrieved TCWV when scattering is neglected as a function of Lambertian surface albedo and aerosol optical thickness at 900 nm for a total columnar water vapour of 56mm, a viewing zenith angle (VZA) of 30°, a solar zenith angle (SZA) of 64° and a relative azimuth angle (RAA) of 0° (≡sensor is placed opposite of sun). In the upper panels, f was calculated for a continental aerosol located in the boundary layer, the lower panels correspond to an aerosol layer in the upper troposphere. Several conclusions can be drawn from the shown plots:

1. The scattering correction factor is close to 1 for bright surfaces because the measurement is dominated by photons that have been reflected at the bottom of the atmosphere, resulting in a small difference between T and T_{noscat}.

2. Above dark surfaces such as the ocean, f is increased, as the predominant part of the detected photons is reflected by atmospheric scatterers and thus does not traverse the whole vertical column of water vapour.

AMTD
4, 6811–6844, 2011

3. Correspondingly, there is a strong bias in retrieved TCWV if scattering is neglected above dark surfaces and a less pronounced effect for bright surfaces (see right panels).

4. Elevated aerosol layers have a much stronger effect on the measured transmittance as compared to scatterers located in the boundary layer (see lower panels).

One of the most important parameters determining f is thus the surface albedo. Figure 2 shows global histograms of land surface albedo at 900 nm throughout the year 2004, as extracted from the MERIS Albedomap (Muller et al., 2007), providing 16-day averages of surface albedo in the MERIS bands on a $0.05^{\circ} \times 0.05^{\circ}$ longitude-latitude grid. In the near infrared spectral region the land surface reflectance is commonly larger than 0.2. In case of boundary layer aerosols, this corresponds to a bias of 10–30 % in TCWV if scattering is neglected. For a dark ocean surface, the bias is in the range of 50 %. In the less common case of highly elevated aerosols, these values are significantly higher. By applying the scattering correction factor to the modelled transmittance, the bias in retrieved TCWV is eliminated. However, due to uncertainties in auxiliary parameters such as the surface reflectance and the prevailing aerosol type, optical thickness and vertical distribution, a residual uncertainty remains. Due to the significantly stronger influence of scattering above dark surfaces, the resulting uncertainty of the derived water vapour column is much higher above the ocean. Over dark ocean areas (TOA reflectance < 0.1), the true ocean surface reflectance is calculated from the wind speed and the observing geometry (Cox and Munk, 1954; Koepke, 1984). The difference between TOA reflectance and calculated ocean surface reflectance is then used to estimate the aerosol loading and hereupon calculate the scattering correction factor f. This procedure is neither possible nor necessary when the sensor is directed towards the direct glitter of the sun, where the influence of the scattering atmosphere is weak and a climatological value of aerosol optical thickness can be used for the calculation of f.

AMTD
4, 6811–6844, 2011

Figure 3 shows the angular dependence of f for fixed values of AOT (0.28) and surface albedo (0.4). The main statement here is, that the effect of atmospheric scattering on the measured band ratio is more pronounced for high zenith angles and there is an additional influence of the relative azimuth distance between sensor and sun. It is therefore mandatory to include the observation geometry with sufficient angular resolution in the pre-calculated look-up tabels of f.

3.2 Inversion technique

In the retrieval scheme the first guess of TCWV is obtained from a simple regression, relating TCWV to a third order polynomial of ln(R), where the regression coefficients were determined using radiative transfer simulations with MOMO. In the iterative optimization routine, there is a single variable to be fitted, the total columnar water vapour, using a single piece of information, the MERIS band ratio R, with a monotonous relation between both figures. The use of background information about TCWV such as e.g. NWP reanalysis data is therefore not necessary over sufficiently bright targets, as it only dilutes the high sensitivity inherent to the MERIS measurement. The straightforward optimization of TCWV is performed by the secant method. It was preferred to the Newton method in spite of its slightly slower convergence, because there is no need to calculate the derivative of the cost function at every retrieval step, so its implementation provides a faster processing in practice.

Starting with the first guess, TCWV is adjusted until the cost function, represented by the absolute difference between simulated and measured ratio of normalized radiances in MERIS bands 15 and 14, is below a pre-defined threshold, determined by e.g. the sensor noise.

3.3 Uncertainty estimate

Once the iteration procedure has converged the retrieval uncertainty is calculated, taking into account direct measurement errors, that is instrumental noise, as well as the

AMTD
4, 6811–6844, 2011

uncertainties of all those parameters that are not part of the state vector but are fixed a priori. These are the surface albedo and its spectral dependency, the temperature profile, the surface pressure, the aerosol optical thickness and the aerosol height. The uncertainty introduced by these modelling parameters b_i is determined by converting the individual error contributions into measurement space via the modelling parameter Jacobian K_b and adding them to the measurement error covariance matrix S_ϵ, which in our case is just a scalar, as we are only using one piece of information, namely the band ratio R:

$$S_y = S_\epsilon + K_b^T S_b K_b \tag{3}$$

The resulting error covariance matrix S_y, again in our case just a scalar variance of R due to all measurement and model parameter uncertainties, is converted into parameter space using the Jacobian K, that is the partial derivative of the band ratio R with respect to TCWV at the retrieved state. As a result we get $\hat{S}$, the variance of the retrieved state, that is directly used to define the measurement uncertainty (Rodgers, 2000):

$$\hat{S} = (K^T S_y^{-1} K)^{-1} \tag{4}$$

In particular, the contributions of the individual error sources to the uncertainty of the retrieved state are estimated as follows. As detailed in Sect. 3.1, among the above parameters there are 3 candidates affecting the scattering correction factor f, namely the absolute surface reflectance, the aerosol optical thickness and the aerosol height. For each of these parameters, an f_i^* (with $i = 1,2,3$) is calculated from the look-up tables, by perturbing the input accordingly. The perturbance value is 0.1 in case of aerosol optical thickness and 0.02 for the surface albedo. Since there is no information about the vertical distribution of the aerosols, a large error is assumed by shifting the aerosol layer to the uper troposphere instead of locating it in the boundary layer. Instead of f, the f_i^* are used to correct the simulated transmittance for scattering, in each case resulting in a perturbed band ratio R_i^*. We obtain the deviation of the modelled band

AMTD
4, 6811–6844, 2011

ratio $\Delta R_i = |R_i^* - R|$ for each of the three parameters, that are squared and added to the measurement error variance S_ϵ.

In case of surface pressure and temperature, the forward model is used directly to simulate perturbed transmittances that are corrected with an unperturbed scattering correction factor f. The assumed uncertainties are 10 hPa for surface pressure and 5 K for the surface temperature, resulting again in values of $(\Delta R_i)^2$ that are added to S_ϵ.

Above land, the uncertainty introduced by the spectral albedo slope is parameterized with the normalized differenced vegetation index (NDVI) of the observed scene. As shown in Fig. 4, the linear extrapolation of $\alpha_{865\,\mathrm{nm}}$ and $\alpha_{885\,\mathrm{nm}}$ towards 900 nm is a good approximation for vegetated surfaces with an NDVI around 0.6 and less accurate for e.g. bare soils or snow covered areas. Therefore, the NDVI is used to estimate the uncertainty of $\alpha_{900\,\mathrm{nm}}$, ranging from 0.001 to 0.003 for snow-free areas up to 0.006 above snow and ice. Similar to the approach detailed above, a perturbed transmittance is calculated from the perturbed albedo slope using the forward model, with the resulting deviation contributing to S_ϵ. As there is no spectral albedo slope above ocean, no error contribution is calculated here.

The final contribution to S_ϵ is the sensor noise with an assumed signal-to-noise-ratio of 250.

The resulting overall uncertainty of the retrieved TCWV is large over dark targets, where the unknown aerosol vertical distribution is the predominant contributor to the retrieval uncertainty. Over non-vegetated land areas and especially ice and snow-covered regions, the spectral albedo slope uncertainty is an important error contribution.

4 Validation

The MERIS TCWV retrieval was thoroughly validated by comparing it to ground-based reference data over land and satellite-borne microwave retrievals from SSM/I and ENVISAT MWR over ocean. Over land, other than a generally high accuracy, a systematic

AMTD
4, 6811–6844, 2011

wet bias of up to 10 % was observed when comparing MERIS TCWV to the various validation data sets. Provided that there is no dry bias in the used validation data, a potential underestimation of the absorption by water vapour around 900nm was identified as a possible source of this bias. The water vapour absorption is usually described as a sum of absorption lines, that are cut off at a line-width-dependent spectral distance from the line centre, and an underlying, spectrally slowly varying continuum absorption. However, the strength of the continuum absorption and the optimal line wing cut-off are still under discussion, resulting in an uncertain water vapour optical depth. The observed bias in MERIS TCWV is well within this uncertainty, as demonstrated in Sect. 4.3.

Due to fact that the behaviour of the water vapour continuum is not yet well understood, all validation results shown in Subsects. 4.1 and 4.2 are solely based on HITRAN 2008 absorption line parameters (Rothman et al., 2009), hereby neglecting continuum absorption. In order to compensate for not considering continuum absorption, the line wings were not cut off.

4.1 Validation over land

The MERIS TCWV retrieval was thoroughly validated over land against various sources of reference data, namely GUAN radiosonde data, AERONET sunphotometer measurements, ARM microwave radiometer observations and ground-based GPS water vapour monitoring data. For each of these 4 reference data sets, 3 yr of data in the period 2003–2005 were compared to the MERIS retrieval. The results for each data set are shown in Fig. 6 as normalized, color-coded frequency-of-occurence plots. In each plot, the relative frequency of occurrence is shown in grey shading for the whole data set and overplotted in color for a subset, filtered for cloud contamination, high aerosol loading or other disturbing influences. In the top left corner of each panel the sample size, bias, root mean square deviation (in the following rmsd) and the offset and slope of the linear best fit are given for both subsets.

AMTD
4, 6811–6844, 2011

For the comparison of the satellite observations and the particular ground-based reference data sets, MERIS measurements were spatially averaged in order to account for e.g. the radiosonde displacement, the time gap between satellite overpass and ground-based measurement, and the limited accuracy of the MERIS geolocation. Here the value $TCWV_i$ of each considered pixel was weighted with its associated uncertainty σ_i^2: $\sum_{i=0}^{n} w_i * TCWV_i / \sum_{i=0}^{n} w_i$, with $w_i = 1/\sigma_i^2$.

4.1.1 Validation against Aeronet sun photometer measurements (2003–2005)

The MERIS TCWV retrieval was compared to a 3-yr global set of Aeronet sun photometer measurements (see Fig. 5 for Aeronet site locations and top left panel in Fig. 6 for validation results). In order to account for the differing viewing geometries, the time gap between the Aeronet and the MERIS measurements, constrained to ≤30 min, and the limited accuracy of the MERIS geolocation, the MERIS measurements were averaged within 10 km × 10 km, centered around the Aeronet station. As an additional constraint, the measurements were rejected in case there were less than 20 valid MERIS pixels (20 %).

The filtered subset was additionally screened for high aerosol loadings, undetected clouds and outliers, deviating by more than 3σ. The resulting values are a wet bias of MERIS of 1.9 mm and a bias-corrected rmsd of 3.7 mm. In view of the comparisons to microwave radiometer, GPS and radiosondes (bias ≤ 1 mm), the relatively large bias can in parts be explained with a dry bias of the Aeronet sun photometer measurements. The linear fit has a slope of 1.08 and an offset close to 0, meaning that on average MERIS TCWV is 8 % larger than Aeronet TCWV.

4.1.2 Validation against GUAN radiosonde data (2003–2005)

A 3-yr global set of GUAN (GCOS Upper Air Network) radiosonde data was used to compare with the MERIS TCWV retrieval (see Fig. 5 for GUAN site locations and top

AMTD
4, 6811–6844, 2011

right panel in Fig. 6 for validation results). In order to account for the displacement of the radiosonde during its ascent, the time gap between the GUAN and the MERIS measurements, constrained to ≤30 min, and the limited accuracy of the MERIS geolocation, the MERIS measurements were averaged within 40 km × 40 km, centered around the GUAN station. Each contributing MERIS pixel was weighted with its associated uncertainty.

In the subset, filtered for outliers (deviation $\geq 3\sigma$), and cloud contamination, a bias of 1 mm and a bias-corrected rmsd of 2.7 mm are found. These values are within the range of the radiosonde uncertainty. The linear fit shows a slope of 1.04 and an offset of 0.85 mm.

4.1.3 Validation against ARM microwave radiometer data (2003–2005)

A 3-yr set of ground-based ARM Southern Great Plains (SGP) microwave radiometer (MWR) data was used to compare with the MERIS TCWV retrieval (see Fig. 5 for ARM SGP site location and bottom left panel in Fig. 6 for validation results). The MWR instruments are microwave radiometers designed to measure the radiation emitted by atmospheric water vapour and liquid water at frequencies of 23.8 GHz and 31.4 GHz (Turner et al., 2007). Since there is no uncertainty introduced by the background emission of the cold space, ground-based microwave data is considered as one of the most accurate methods for the determination of the water vapour colum amount.

For the comparison, the cloud-free and valid MERIS pixels were averaged within 10 km × 10 km around the ARM sites. The MWR measurements, provided minute-by-minute, were averaged in a ±15 min time frame around the ENVISAT overpass. This averaging was performed in order to minimize disturbing effects such as undetected clouds, inaccurate MERIS geolocation and the different observing geometries.

The comparison of MERIS and MWR TCWV values shows an almost perfect agreement with a wet bias of 0.9 mm and a root mean square deviation of merely 1.3 mm. Apart from the fact that the comparison is limited to the ARM SGP site and is therefore not representative for global observations, this result indicates that the accuracy

AMTD
4, 6811–6844, 2011

of MERIS TCWV over land is outstanding. The wet bias and the linear fit slope of 1.04 indicate again, that the gaseous absorption of water vapour was potentially underestimated.

4.1.4 Validation against ground-based GPS data (2003–2005)

Finally, a 3-yr set of ground based GPS water vapour monitoring data was used to compare with the MERIS TCWV retrieval (see Fig. 5 for GPS site locations and bottom right panel in Fig. 6 for validation results). The analysis of the temperature- and humidity-dependent delay of the GPS signal emitted by satellites and received by ground stations allows the retrieval of TCWV (Bender and Raabe, 2007). In a comparison against microwave radiometer measurements a bias of 1.2 mm and a root mean square deviation of 6 mm was found (Bender et al., 2008).

Again, MERIS measurements were averaged over 10 km × 10 km to account for temporal gaps and the differences in observing geometries. A relatively large portion of points, sitting in the lower right part of the plot, is due to failing cloud detection over snow covered parts of Germany in winter. After filtering out these cases, a bias of 0.6 mm and a rmsd of 2.1 mm results. In accordance with the results of the comparisons against the other reference data sets, the linear fit has a slope of 1.09 and an offset of −0.63 mm.

4.2 Validation over ocean

4.2.1 Validation against SSM/I microwave data

The Special Sensor Microwave/Imager (SSM/I) is a passive, seven-channel, four-frequency microwave radiometer which is operated on the DMSP (US Air Force Defense Meteorological Satellite Program) satellite series. Depending on the channel, SSM/I has a footprint of several tens of kilometers. Due to the well known emissivity of the water surface and the high radiometric accuracy of the instrument (0.4–0.7 K),

AMTD
4, 6811–6844, 2011

SSM/I-derived TCWV is regarded as one of the most accurate water vapour data sets available over ocean. The data used for the comparison stems from the F13 and F14 satellites with a local equator crossing time in the early morning. Both the time gap of 4–5 h between SSM/I and MERIS observations and the fact that microwave observations of TCWV are possible under all sky conditions whereas MERIS provides only cloud-free measurements have to be taken into account for the interpretation of the results.

In order to account for the differences in footprint and overpass time, both data sets were averaged within 0.5° × 0.5° boxes. Cases with less than 30 % of valid MERIS pixels within a box were excluded from the analysis. The accuracy of the MERIS water vapour retrieval is expected to depend on the reflectance of the ocean surface, as over the dark ocean the signal is dominated by the aerosol height and optical depth whereas the unknown impact of atmospheric scattering is less important over bright targets. Due to the forenoon orbit of ENVISAT and the observing geometry of MERIS, direct reflection of the incoming sun light occurs in the eastern part of the MERIS swath, whereas the central and western parts of the MERIS swath are mainly covered by dark ocean. The left panel of Fig. 7 shows the relative frequency of occurence for the comparison of MERIS and SSM/I derived TCWV in the 0.5° × 0.5° boxes. As in the land validation plots, the background, gray shaded distribution represents a moderately filtered data volume (30 % valid MERIS pixels and standard deviation less than 5 mm in 0.5° × 0.5° box) whereas the foreground, color coded distribution represents a more strictly filtered data volume over the brighter parts of the ocean (30 % valid MERIS pixels and standard deviation less than 2 mm in 0.5° × 0.5° box, cloudy cases excluded, ocean reflectance $\rho \geq 0.08$). The root mean square deviation between $TCWV_{MERIS}$ and $TCWV_{SSM/I}$ is 8.6 mm for the moderately filtered cases and drops to 5.2 mm for the stricter filtering. The bias of −0.3 mm, influenced by undetected clouds, is modified to 2.5 mm, accordingly. Although there is a time gap of 4–5 h between both measurements and the foot prints and measurement techniques differ, the relatively large bias hints at deficiencies of the MERIS retrieval. Apart from the potential underestimation of optical depth for a

AMTD
4, 6811–6844, 2011

given water vapour colum amount, a possible source for the strong wet bias could be the scattering correction factor, that is calculated for a Lambertian surface, which is a good approximation for most land surfaces but not applicable over ocean.

4.2.2 Validation against ENVISAT MWR data

The ENVISAT microwave radiometer (MWR) is a passive, dual-channel, nadir-pointing radiometer, operating at frequencies of 23.8 GHz and 36.5 GHz. Its primary objective is to support the tropospheric path correction of the ENVISAT radar altimeter signal by measurements of the atmospheric humidity over ocean (Obligis et al., 2006). The MWR has a 20 km × 20 km footprint at nadir, so only the central part of the MERIS swath can be compared to MWR data. As sun glint is found mainly in the eastern part of the MERIS swath, the comparison is limited to the darker parts of the ocean, where MERIS is expected to perform less accurately. Besides, as MWR provides only two channels, its accuracy is expected to be reduced as compared to SSM/I data. On the other hand, there is no time gap between MWR and MERIS observations.

Figure 7 (right panel) shows the direct comparison between MWR and MERIS TCWV for four months (October and November 2002 and June and July 2007) of global observations over ocean. MERIS measurements were averaged over 20 km × 20 km in order to match the MWR footprint and excluded in case less than 25 % of the MERIS pixels were valid within this box. The scatter plot shows the relative frequency of occurrence of all resulting cases in gray shading, overplotted with a subset of cases coded in color. The cases occurring in the lower right corner of the diagram and those 20 km × 20 km boxes with a high standard deviation of MERIS TCWV were filtered out for the subset in order exclude cloudy cases that were falsely classified as clear sky by the MERIS cloud mask. The analysis of the filtered data revealed a bias of 3.1 mm between MERIS and MWR with a bias-corrected root mean square deviation of 5.1 mm. This result is in accordance with the validation of MERIS TCWV against SSM/I observations.

AMTD
4, 6811–6844, 2011

4.3 Sensitivity to water vapour continuum absorption

The spectral structure and strength of the absorption of solar radiation by atmospheric water vapour is commonly described by the Voigt line profile, defining the dependence of the line strength, shape and width as a function of pressure and temperature. The Voigt profile is known to accurately describe the absortion close to the line centres, but to result in a suboptimal description of the far wings of the lines. It is therefore common to cut off the line wings at a certain spectral distance from the line centres and describe the residual absorption and other spectrally slowly varying effects, such as the absorption due to water vapour dimers, by a water vapour continuum model. Although the water vapour continuum is much smaller in the NIR as compared to the thermal regions, it still has a significant influence on the resulting total gaseous optical depth. In the frame of this work, the widely used LBLRTM code (Clough et al., 2005) was used to calculate the absorption by water vapour, embodying the MT-CKD model for the description of the continuum absorption. However, recent publications such as the paper by Ptashnik et al. (2011), indicate that the strength of the continuum absorption is still highly uncertain, giving rise to the question whether the systematic wet bias observed in the validation of the MERIS TCWV retrieval is caused by an underestimation of the water vapour absorption.

Figure 8 shows the effect of adding the continuum absorption on the spectral structure of the gaseous optical depth in a spectral window between 895 nm and 905 nm for four different setups:

1. Line wings are cut off at a spectral distance of 64 times the full width at half maximum (fwhm) of each line and no continuum optical depth is added.
2. as for setup 1, but a MT-CKD continuum is added.
3. as for setup 1, but a doubled MT-CKD continuum is added.
4. the line wings are not cut off and no continuum is added.

AMTD
4, 6811–6844, 2011

The lower right plot shows the equivalent change of TCWV for the four different setups, relative to the common approach (setup 2). If the continuum is neglected (setup 1), an overestimation of up to 20 % of TCWV results. Accordingly, adding a doubled continuum results in an underestimation of similar magnitude. Note that the relative overestimation is stronger for high values of TCWV, meaning that the continuum has a stronger effect in case of humid atmospheres. When the line wing cutoff is not performed and no continuum is added, the resulting optical depth is higher than for the common approach, but lower than adding a doubled continuum. Note that all shown configurations result in a wet bias of MERIS, except for setup 4, that results in a perfect fit against e.g. ground-based MWR observations.

The observed wet bias of MERIS TCWV is in close agreement with validation results obtained by Gao and Kaufman (2003) for near infared measurements of the Moderate Resolution Imaging Spectroradiometer.

5 Summary and outlook

We present a new algorithm for the retrieval of TCWV from MERIS measurements in the $\rho\sigma\tau$-absorption band in the near infrared spectral range. It is based on fast forward simulation of the absorption by water vapour, corrected for the difference in surface albedo between the used MERIS bands and the impact of atmospheric scattering on the measured band ratio. The forward operator takes into account the temperature- and pressure-dependence of the absorption lines. The algorithm provides realistic uncertainty estimates on a pixel-by-pixel basis, considering all relevant error sources of uncertainty, including instrumental noise as well as forward model parameter uncertainties. The retrieved data is thus well qualified for the generation of level 3 products such as global time series.

Over land, an extensive validation study against various sources of ground based reference data sets generally revealed a high accuracy of MERIS TCWV with bias-corrected root mean square deviations of 3.7 mm (Aeronet sun photometer

AMTD
4, 6811–6844, 2011

measurements), 2.7 mm (GUAN radiosondes), 1.3 mm (ARM MWR measurements) and 2.1 mm (German ground-based GPS data). In all comparisons a wet bias of MERIS TCWV between 0.6 mm (GPS), 1 mm (ARM MWR and GUAN radiosondes) and 1.9 mm (Aeronet) was found. A potentially improper description of the water vapour continuum absorption is a possible explanation for this wet bias, especially in view of the fact that similar effects have been observed for MODIS observations in the near infrared spectral range (Gao and Kaufman, 2003). It was shown that the MERIS bias is within the range of this spectroscopic uncertainty. A different, possible explanation for the observed wet bias could be the instrument calibration, such as e.g. overcorrected instrumental stray light, as observed in the MERIS oxygen A band channel for some parts of the field of view (Lindstrot et al., 2010).

The MERIS TCWV retrieval was validated over ocean using coincident ENVISAT MWR data and SSM/I observations. Both comparisons showed a wet bias of 2–3 mm, hinting at deficiencies in the description of the radiative interaction between atmosphere and ocean surface. The bias-corrected root mean square deviation between MERIS and MWR and SSM/I is in the range of 5 mm, which is a reasonable value, given the uncertainty of the atmospheric scattering component over ocean.

In the frame of the ESA DUE GlobVapour project, the presented MERIS TCWV algorithm was used above land and coastal waters and combined with SSM/I derived TCWV above open ocean for a generation of a global time series. The Ocean and Land Colour Instrument (OLCI) onboard the Sentinel-3 satellite will continue the MERIS measurements during the next decades.

Acknowledgements. This work was performed in the frame of the ESA DUE GlobVapour project (ESRIN/AO/1-6090/09/I-OL). The ENVISAT MWR data was provided by CLS in the frame of its RA2-MWR ESL L1b activities (ESA contract ENVI-SPPA-EOPG-SW-10-0034). The authors would like to thank Bruno Picard of CLS for providing the ENVISAT MWR data and Marc Schröder of Deutscher Wetterdienst for providing SSM/I data.

AMTD
4, 6811–6844, 2011

References

Albert, P., Bennartz, R., Preusker, R., Leinweber, R., and Fischer, J.: Remote Sensing of Atmospheric Water Vapor Using the Moderate Resolution Imaging Spectroradiometer (MODIS), J. Atmos. Ocean. Tech., 22, 309–314, 2005. 6813

Bender, M. and Raabe, A.: Preconditions to ground-based GPS water vapour tomography, Ann. Geophys., 25, 1727–1734, 2007, http://www.ann-geophys.net/25/1727/2007/. 6827

Bender, M., Dick, G., Wickert, J., Schmidt, T., Song, S., Gendt, G., Ge, M., and Rothacher, M.: Validation of GPS slant delays using water vapour radiometers and weather models, Meteorol. Z., 6, 807–812, 2008. 6827

Bennartz, R. and Fischer, J.: A modified k-distribution approach applied to narrow band water vapour and oxygen absorption estimates in the near infrared, J. Quant. Spectrosc. Radiat. Transfer, 66, 539–553, 2000. 6817

Bennartz, R. and Fischer, J.: Retrieval of columnar water vapour over land from back-scattered solar radiation using the Medium Resolution Imaging Spectrometer (MERIS), Remote Sens. Environ., 78, 271–280, 2001. 6813

Clough, S. A., Shephard, M. W., Mlawer, E. J., Delamere, J. S., Iacono, M. J., Cady-Pereira, K., Boukabara, S., and Brown, P. D.: Atmospheric radiative transfer modeling: a summary of the AER codes, Short Communication, J. Quant. Spectrosc. Radiat. Transfer, 91, 233–244, 2005. 6830

Cox, C. and Munk, W.: Measurement of the Roughness of the Sea Surface from Photographs of the Sun's Glitter, J. Opt. Soc. Am., 44, 838–850, 1954. 6819, 6820

Delwart, S., Preusker, R., Bourg, L., Santer, R., Ramon, D., and Fischer, J.: MERIS inflight spectral calibration, Int. J. Remote Sens., 28, 479–496, 2007. 6817

Fell, F. and Fischer, J.: Numerical simulation of the light field in the atmosphere-ocean system using the matrix-operator method, J. Quant. Spectrosc. Radiat. Transfer, 3, 351–388, 2001. 6819

Fischer, J.: High-resolution spectroscopy for remote sensing of physical cloud properties and water vapour, in: Current problems in atmospheric radiation (pp. 151-156) edited by: Lenoble, J. and Geleyn, J.-F., Hampton, Virginia, USA: Deepak Publishing, 1988. 6815

Fischer, J. and Grassl, H.: Radiative transfer in an atmosphere-ocean system: an azimuthally dependent matrix-operator approach, Appl. Opt., 23, 1035–1039, 1984. 6819

AMTD
4, 6811–6844, 2011

Gao, B.-C. and Kaufman, Y. J.: Water vapor retrievals using Moderate Resolution Imaging Spectroradiometer (MODIS) near-infrared channels, J. Geophys. Res., 108, 4389, doi:10.1029/2002JD003023, 2003. 6813, 6831, 6832

Heise, S., Wickert, J., Beyerle, G., Schmidt, T., and Reigber, C.: Global monitoring of tropospheric water vapor with GPS radio occultation aboard CHAMP, Adv. Space Res., 37, 2222–2227, doi:10.1016/j.asr.2005.06.066, 2006. 6813

Koepke, P.: Effective reflectance of oceanic whitecaps, Appl. Opt., 23, 1816–1824, 1984. 6819, 6820

Lindstrot, R., Preusker, R., and Fischer, J.: The empirical correction of stray light in the MERIS oxygen A band channel, J. Atmos. Ocean. Technol., 27, 1185–1194, 2010. 6817, 6832

McClatchey, R., Fenn, R., Selby, J., Volz, F., and Garing, J.: Optical Properties of the Atmosphere, Air Force Cambridge Research Laboratories, 3rd Edn., 1972. 6818

Muller, J.-P., Preusker, R., Fischer, J., Zuhlke, M., Brockmann, C., and Regner, P.: ALBEDOMAP: MERIS land surface albedo retrieval using data fusion with MODIS BRDF and its validation using contemporaneous EO and in situ data products, in: IGARSS Int. Geosci. Remote Se., 2007, 2404–2407, doi:10.1109/IGARSS.2007.4423326, 2007. 6820, 6838

Noël, S., Buchwitz, M., Bovensmann, H., and Burrows, J. P.: Retrieval of total water vapour column amounts from GOME/ERS-2 data, Adv. Space Res., 29, 1697–1702, 2002. 6813

Obligis, E., Eymard, L., Tran, N., Labroue, S., and Femenias, P.: First three years of the microwave radiometer aboard ENVISAT: In-fight calibration, processing, and validation of the geophysical products, J. Atmos. Ocean. Technol., 23, 802–814, 2006. 6829

Pougatchev, N., August, T., Calbet, X., Hultberg, T., Oduleye, O., Schlüssel, P., Stiller, B., Germain, K. St., and Bingham, G.: IASI temperature and water vapor retrievals - error assessment and validation, Atmos. Chem. Phys., 9, 6453–6458, doi:10.5194/acp-9-6453-2009, 2009. 6813

Ptashnik, I. V., Shine, K. P., and Vigasin, A. A.: Water vapour self-continuum and water dimers: 1. Analysis of recent work, J. Quant. Spectrosc. Ra., 112, 1286–1303, 2011. 6830

Rast, M., Bezy, J. L., and Bruzzi, S.: The ESA Medium Resolution Imaging Spectrometer MERIS – A review of the instrument and its mission, Int. J. Remote Sens., 20, 1681–1702, 1999. 6813

Rodgers, C.: Inverse Methods for Atmospheric Sounding: Theory and Practice, World Scientific, London, 2000. 6822

AMTD
4, 6811–6844, 2011

Rothman, L., Gordon, I., Barbe, A., Benner, D., Bernath, P., Birk, M., Boudon, V., Brown, L., Campargue, A., Champion, J.-P., Chance, K., Coudert, L., Dana, V., Devi, V., Fally, S., Flaud, J.-M., Gamache, R., Goldman, A., Jacquemart, D., Kleiner, I., Lacome, N., Lafferty, W., Mandin, J.-Y., Massie, S., Mikhailenko, S., Miller, C., Moazzen-Ahmadi, N., Naumenko, O., Nikitin, A., Orphal, J., Perevalov, V., Perrin, A., Predoi-Cross, A., Rinsland, C., Rotger, M., Simeckova, M., Smith, M., Sung, K., Tashkun, S., Tennyson, J., Toth, R., Vandaele, A., and Auwera, J. V.: The HITRAN 2008 molecular spectroscopic database, J. Quant. Spectrosc. Radiat. Transfer, 110, 533–572, doi:10.1016/j.jqsrt.2009.02.013, 2009. 6824

Schlüssel, P. and Emery, W. J.: Atmospheric water vapour over oceans from SSM/I measurements, Int. J. Remote Sens., 11, 753, doi:10.1080/01431169008955055, 1990. 6813

Susskind, J., Barnet, C. D., and Blaisdell, J. M.: Retrieval of atmospheric and surface parameters from AIRS/AMSU/HSB data in the presence of clouds, IEEE T. Geosci. Remote Sens., 41, 390–409, 2003. 6813

Turner, D. D., Clough, S. A., Liljegren, J. C., Clothiaux, E. E., Cady-Pereira, K., and Gaustad, K. L.: Retrieving liquid water path and precipitable water vapor from Atmospheric Radiation Measurement (ARM) microwave radiometers., IEEE T. Geosci. Remote Sens., 45, 3680–3690, doi:10.1109/TGRS.2007.903703, 2007. 6826

AMTD
4, 6811–6844, 2011

Table 1. Central wavelength and bandwidth (fwhm) of MERIS spectral channels.

Band	Center (nm)	Width (nm)	Usage
1	412.5	10	Yellow substance, turbidity
2	442.5	10	Chlorophyll
3	490	10	Chlorophyll, pigment
4	510	10	Suspended matter, turbidity
5	560	10	Chlorophyll, suspended matter
6	620	10	Suspended matter
7	665	10	Chlorophyll
8	681.25	7.5	Chlorophyll
9	708.25	10	Atmospheric correction, "red edge"
10	753.75	7.5	Cloud optical thickness, cloud-top pressure reference
11	761.75	3.75	Cloud-top pressure
12	778	10	Aerosol, vegetation
13	865	20	Aerosol, atmospheric correction
14	885	10	Water vapour reference
15	900	10	Water vapour

AMTD
4, 6811–6844, 2011

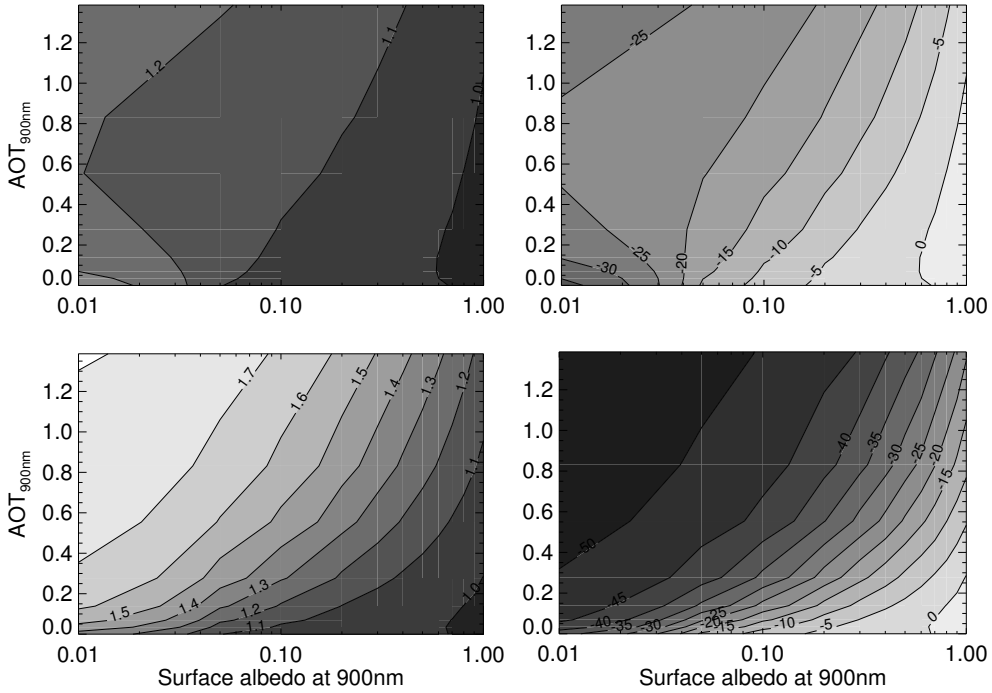

Fig. 1. Scattering correction factor depending on surface albedo and aerosol optical thickness at 900 nm (left panels) and equivalent underestimation of TCWV in mm when scattering is neglected (right panels), shown for SZA = 64°, VZA = 30°, RAA = 0°, TCWV = 56 mm and a continental aerosol located in the boundary layer (upper panels) and the upper troposphere (lower panels), respectively.

AMTD
4, 6811–6844, 2011

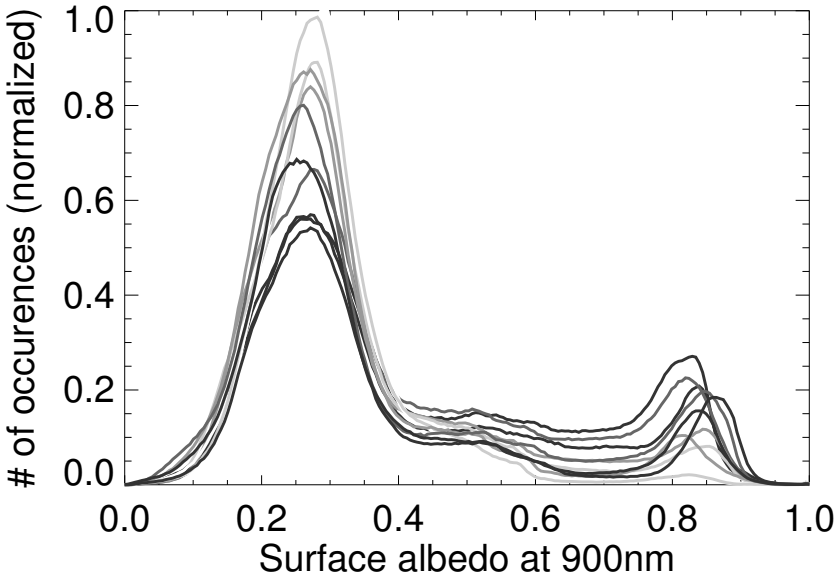

Fig. 2. Global, normalized histograms of surface reflectance at 900 nm through the year 2004 (grey shading indicating seasonal dependence with dark grey indicating winter and light grey indicating summer months). The data was extracted from the MERIS Albedomap data set (Muller et al., 2007).

AMTD
4, 6811–6844, 2011

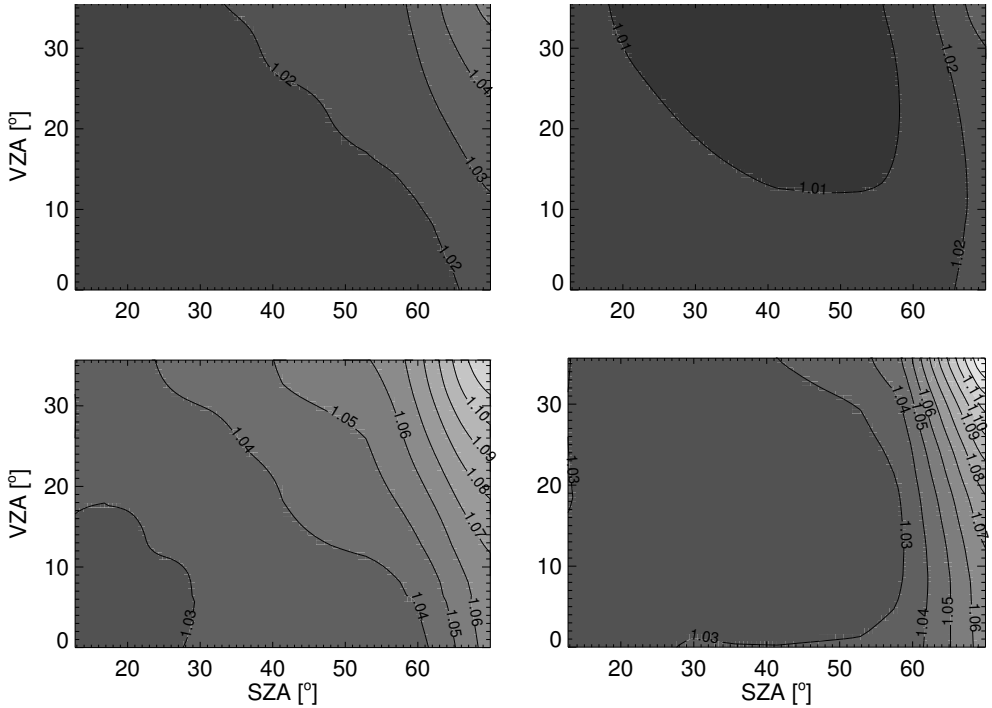

Fig. 3. Scattering correction factor depending on viewing and illumination geometry for relative azimuth angle of 180° (left panels) and 0° (right panels), with 0° representing cases where the sensor is placed opposite of the sun, shown for aerosol optical thickness of 0.28, a surface albedo of 0.4, TCWV of 56 mm and a continental aerosol located in the boundary layer (upper panels) and the upper troposphere (lower panels), respectively.

AMTD
4, 6811–6844, 2011

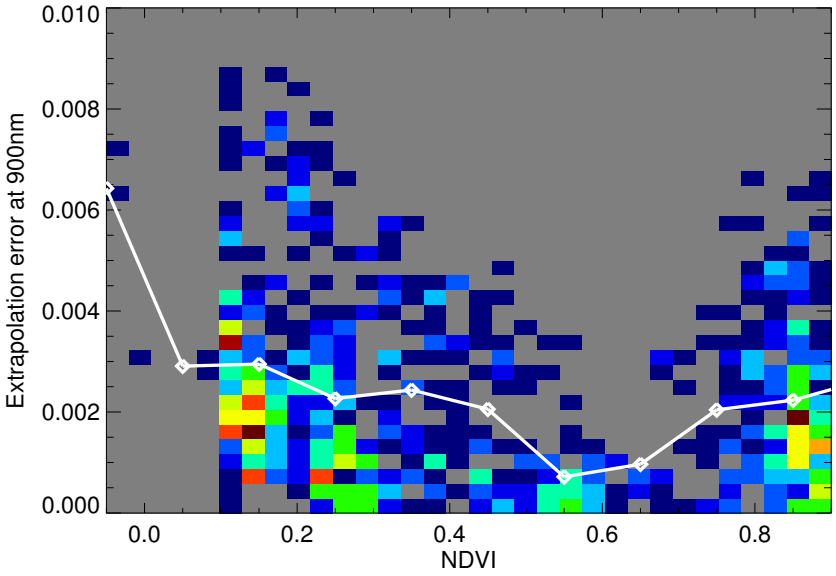

Fig. 4. Normalized frequency of distribution of error of linearly extrapolated surface albedo at 900 nm (color coded) and resulting error parameterization (white curve) as a function of NDVI .

AMTD
4, 6811–6844, 2011

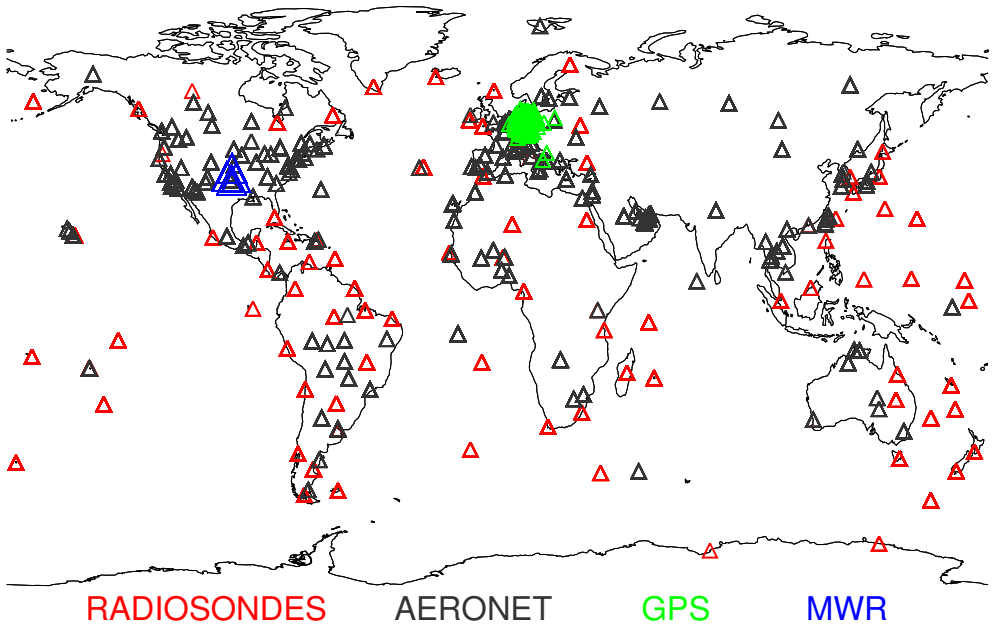

Fig. 5. Geographic distribution of used validation data over land.

AMTD
4, 6811–6844, 2011

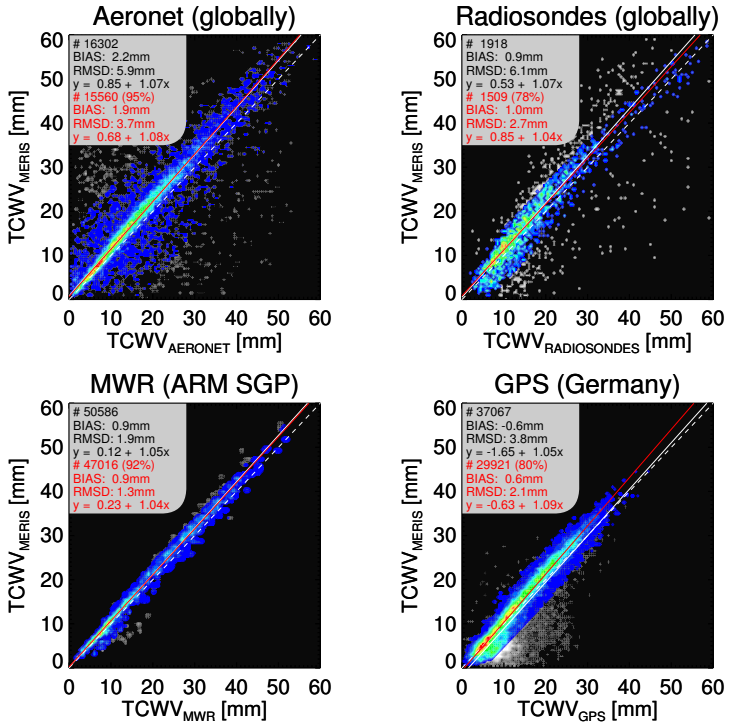

Fig. 6. Normalized frequencies of occurrence for comparisons of MERIS-derived TCWV against AERONET sun-photometer measurements (top left), GUAN radiosondes (top right), ARM Southern Great Plains microwave radiometer data (bottom left) and ground based GPS data (bottom right), each for the period 2003–2005. See Fig. 5 for geographic distribution of validation data and text for detailed discussion.

AMTD
4, 6811–6844, 2011

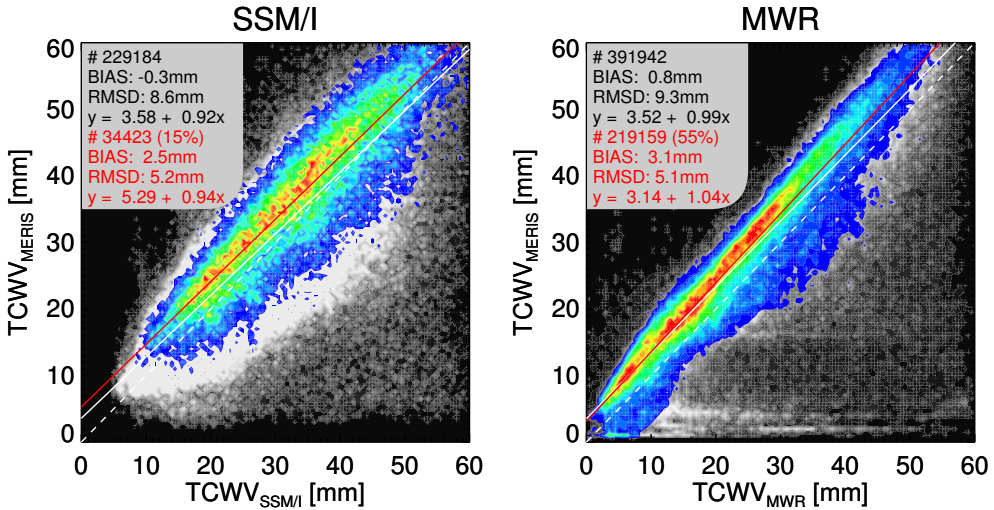

Fig. 7. Left panel: normalized frequency of occurrence for global comparison of SSM/I and MERIS TCWV over ocean (July 2007). Both retrievals were averaged within 0.5° × 0.5° degree boxes in order to account for the differing footprints and different observation times. Right panel: normalized frequency of occurrence for direct, global comparison of ENVISAT MWR amd MERIS TCWV over ocean (October–December 2002, June–September 2007). MERIS measurements were averaged within 20 × 20 km^2 in order to match MWR footprint.
Gray shaded background indicates distribution of compared cases without filtering, with the black text specifying statistical analysis and white solid line representing the linear fit. Color coded foreground indicates the distribution of cases, filtered for undetected clouds (lower right regions), high MERIS uncertainty and dark ocean reflectance ($\rho \geq 0.08$, applied to SSM/I comparison only). See text for more detailed description.

AMTD
4, 6811–6844, 2011

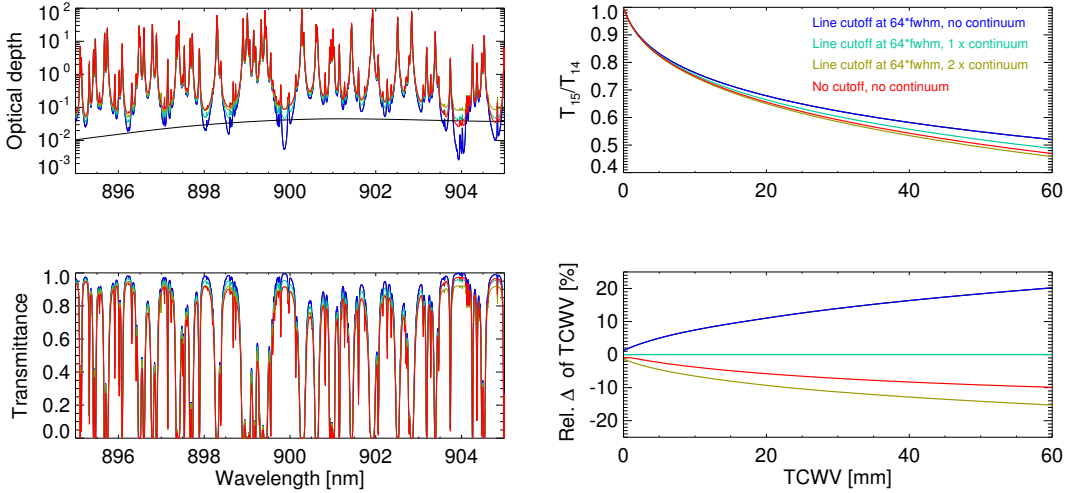

Fig. 8. Left panels: sensitivity of optical depth (upper figure) and transmittance (lower figure) at 900 nm to spectroscopic assumptions. The colors of the curves denote the underlying line cutoff width and continuum absorption, as indicated in the upper right plot. The continuum optical depth is shown in black in the upper left panel. Right panels: transmittance ratio of MERIS bands 15 and 14 as a function of TCWV (upper) and corresponding relative difference of derived TCWV, in relation to retrieval based on line cutoff at 64*fwhm and a MT-CKD continuum. All shown results were calculated for a mid-latitude summer atmosphere, a surface pressure of 1050hPa and an airmass of 3.

AMTD
4, 6811–6844, 2011